Available online at www.sciencedirect.com

ScienceDirect

Journal of Magnesium and Alloys 8 (2020) 134–149

www.elsevier.com/locate/jma

Review

Formulation of corrosion rate of magnesium alloys using microstructural parameters

Ahmad Bahmani, Srinivasan Arthanari, Kwang Seon Shin*

Magnesium Technology Innovation Center, School of Materials Science and Engineering, Seoul National University, 1 Gwanak-ro, Gwanak-gu, Seoul 08826, Korea

Received 8 July 2019; received in revised form 25 November 2019; accepted 14 December 2019
Available online 30 January 2020

Abstract

Up to the date of writing this article, a quantitative analysis between corrosion rate and combined microstructural parameters including composition, grain size, and precipitations has not been reported. Hence, a literature review was carried out on these parameters to understand the quantitative effect of each one on the corrosion rate of Mg and Mg alloys. Moreover, using the available data in the literature and several experimental results, a new model was developed to predict the corrosion rate, through microstructural parameters. This model suggests that by using ultra-fined grains, alloying compounds with low Volta-potential difference relative to the matrix and a low fraction of secondary phase, a very low corrosion rates of materials are achievable.

Keywords: Corrosion rate; Magnesium; Grain size; Volta-potential.

1. Introduction

The corrosion rate is the rate of corrosion attack to material and is the most straightforward parameter to compare the corrosion behavior of materials. Prediction of the corrosion rate by considering several microstructural parameters of material is still a challenging task. Indeed, several parameters such as intrinsic/extrinsic microstructural parameters and alloying produce complex mechanisms involved in corrosion. Even though the corrosion rate determines the life of components in use and it is one of the most critical parameters in industry, to our knowledge, a relationship between corrosion rate and some affecting microstructural parameters using a model equation have not been previously reported.

Throughout the history of the industry, engineers have always been involved in designing new materials with desired properties. The corrosion rate is one of those properties that limit the application of materials. Magnesium alloys are the most challenging materials because they are very attractive in the industry due to their high strength to weight ratio which makes the components lighter, however, their high corrosion rate restricts their usage. Having the ability to predict the corrosion rates can help researchers and engineers to design the material with the desired corrosion rate without altering much on the mechanical properties. They may also find out the routes of designing stainless magnesium which is very important in large scale applications.

Therefore, in this work, we propose an equation considering how the microstructural parameters can model the corrosion rate. Even though the model has been defined for the magnesium alloys and all studied works have been done in magnesium alloys, but same work can be extended on other alloys and the equation can be generalized for other materials as well.

1.1. Parameters influencing the corrosion behavior

There are several parameters such as composition, grain size (grain boundary), and second phase which mainly determine the corrosion rate of Mg alloys.

* Corresponding author.
E-mail address: ksshin@snu.ac.kr (A. Bahmani).

https://doi.org/10.1016/j.jma.2019.12.001

1.1.1. Alloy composition

The alloy composition has two effects on the corrosion rate such as intrinsic and extrinsic:

1.1.1.1. Intrinsic effect.

- *Surface potential:* Surface potential (surface nobility or weakness) of the matrix can be changed by the dissolution of solutes into the matrix [1]. Further, the surface potential might also be changed by lattice strain (dislocation density), which is related to the deformation conditions. A linear relationship exists between the surface potential and work function which is the minimum energy required to remove an electron from the surface of a material to a point in a vacuum outside the surface. Surface potential can be measured by various techniques such as scanning kelvin probe force microscopy (SKPFM) which is commonly used for several alloys [2,3]. Open circuit potential (OCP) can also be used; however, OCP includes other effects such as grain boundary and second phases. The first principle calculation has also been utilized to measure the work function of the surface [4].
- *Second phases:* The addition of alloying elements produces second phases with different fractions. (This effect will be discussed later).
- *Orientation (Texture Effect):* Here the effect of texture has also been considered as their effect on metal matrix. The corrosion rate of a metal matrix with various crystalline orientations could be affected by changes in alloying composition ($CR_{T,C}$). It is known that the different crystallographic orientations have different corrosion rates. For directionally deformed alloys with intense texture, this parameter needs to be considered. The corrosion rate related to the effect of orientation can be considered as $a_C \times (\Sigma f_{A,or} \times CR_{or})$, where a_C is the effect of solutes and density of dislocations in altering the corrosion rate of grains, and $f_{A,or}$ and CR_{or} are the area fraction of each orientation and corrosion rate of the related orientation, respectively. Several studies have been carried out to understand the effect of texture on the corrosion rate. In fact, since different crystallographic planes have different atomic densities, they show different corrosion rates. In HCP-structured materials, basal planes and after that prismatic II and then prismatic I planes have the highest corrosion resistance compared to other intermediate planes [5–13]. Additionally, it has been reported that any misorientation from the packed planes including basal and prismatic planes increases the corrosion rate [6].

So, it can be seen that the effect of the composition can be considered through a few parameters which affect microstructure, second phase distribution, and their potential difference, or altering the possible passive layer formation.

1.1.1.2. Extrinsic effect (Passivation: $CR_{P,C}$). Passivation is the formation of an outer layer such as metal oxide on the base metal as a micro coating through the chemical reaction of base material with the aqueous environment/electrolyte and it protects the substrate against further corrosion. Passivity in an Mg alloy is achieved by enough concentration of elements such as Ca, Y or Al having the passivating capability in the matrix [14]. Passivation is related to several parameters such as formation Gibbs free energy (or enthalpy in a fixed temperature), cohesive energy which shows overall chemical stability of a material [15], Pilling-Bedworth (PB) ratio which shows the compactness and also coherency of the layer with the substrate. A higher E_{coh} implies that more energy is required to break up the primary chemical bonds. For instance Y, Al and Ca hydroxides have higher cohesive energy than $Mg(OH)_2$, and they can significantly improve the corrosion resistance of alloys [15]. The PB ratio of MgO on the surface is less than 1 (PB $<$ 1) resulting in weak coverage of the surface or forming a porous film [16]. In fact, high-purity Mg is active in all experimental conditions except in chromic acid solution [17,18]. Even though some elements such as Ti, Al and Cr may form oxide films with PB ratio $>$1, but their oxides have high solubility in aqueous solutions. Hence, they cannot usually produce a stable and protective surface film on Mg [14].

1.1.2. Grain size

Grain size is an important factor that determines mechanical properties and corrosion behavior of metals. In the case of mechanical properties, yield strength and hardness are related the grain size through the Hall-Petch equation. However, the effect of grain size on the corrosion rate is more complicated and there are several controversial reports where some reported increase in grain size increases the corrosion rate and some report the opposite.

In order to understand the effect of grain size on the corrosion rate, a literature review was done for various pure metals as well as alloys which are summarized in Table 1. From Table 1, it can be concluded that different relationships and trends between grain size and corrosion rate for both pure materials and alloys can be noticed. Based on the literature, the relationship between grain size and corrosion rate can be classified as:

(i) Increase in grain size decreases the corrosion rate. The reasons could be:
  - Decreasing lattice strain and dislocations density and decreasing the surface potential (at elevated temperatures)
  - Dissolution of second phases into the matrix at elevated temperatures (as a side effect during the heat treatment)
  - Continuous cathodic second phases formed in the casting of alloys (especially with a high concentration of alloying elements and second phase) may break down into several isolated phases within deformation and their role as protection might be changed to several isolated cathodic cells that accelerate the dissolution of the matrix.

(ii) Decrease in grain size decreases the corrosion rate:

Table 1
A literature review on the effect of grain size on corrosion rate.

Grain size, D (μm)	Process	Material	Solution	D decreases ➔ CR ?	How to change D	The mechanism	Ref.
6000– 30	Extrusion	Pure Mg	Hank's	Decreases	Extrusion of cast material (250 °C)	Preferred crystallographic pitting (PCP) was initiated by Fe precipitates in pure Mg and was propagated along with a (0 0 0 1) plane in a grain. Refining the grain size of pure Mg by hot extrusion reduced PCP propagation, indicating that the grain boundaries act as a barrier to pit propagation	[24]
30–20	Extrusion	Pure Mg	3.5 wt.% NaCl	Decreases	Temp. (180, 220, 250 °C)	The film resistance of the pure magnesium sample extruded at 250 °C was the lowest, and the result indicates that magnesium hydroxide film formed on the surface of the sample extruded at higher temperature is thinner or less stable, so that the electrolyte can easier penetrate and promote the continuous dissolution of the pure magnesium	[25]
1000–200	Directional Solidification	Pure Mg	SBF [26]	Decreases	Solidification Rate	Decreasing the corrosion rate at higher solidification rate was attributed to refined grains that can produce more uniform and dense films on the surface of pure magnesium	[23]
1000–11.5	FSP	Pure Mg	SBF	Decreases	Number of passes	Increasing the intensity of basal planes by increasing the number of passes enhances the corrosion resistance and hence decreases the corrosion rate	[27,28]
1500–200	ECAP from Cast	Pure Mg	3.5 wt.% NaCl	Increases	Number of passes	Grain refinement resulted in larger lattice strain and defects and hence deeper pits and higher corrosion rate	[29]
100–2	ECAP	Pure Mg	0.1 M NaCl	Decreases	Number of passes	Increased number density coupled with high misorientated grain boundaries after ECAP promoted a more coherent hydroxide layer on the surface	[20]
1500–9	ECAP	Pure Mg	SBF	Increases (with decreasing processing temperature from 360 to 250 °C) and increases (with decreasing processing temperature from 250 °C to 200 °C)	ECAP Temp.	ECAP introduces several dislocations and lattice defects. A $MgO/Mg(HO)_2$ passive film is probably nucleated on these defects. Introducing more defects by ECAP leads to nucleation of more sites for the formation of film on the substrate	[30]
7.0–0.3	ECAP and Anneal	Pure Ti	HCL-H_2SO_4 (1, 3 and 5 M)	Decreases	ECAPed material was annealed at 80 °C	The corrosion rate decrease after grain refinement is due to rapid passivation of UFG Ti and segregation of impurities on grain boundaries Johansen et al. [31] found that the Ti oxide film formed faster on the surface of 34% plastically deformed samples than that of annealed ones Lower passivation current was found for deformed Ti than for annealed Ti in Tomashov and Ivanov's research [32]. They believed that passivation first started on lattice defects at the exposed surface. UFG Ti has a high density of grain boundaries and dislocations inside grains leading to a high fraction of passive sites and hence, low corrosion rate	[32]
N/A	Severe Rolling	Pure Fe	Na_2SO_4	Decreases	Severe rolling	The main reason for improved corrosion resistance of BNII (Bulk Nano Crystalline Iron Ingot) comparing with CPII (Poly Crystalline Iron Ingot) may be related to the difference between their microstructure and texture. The orientation ⟨111⟩ (110) was dominant and this texture has been enhanced after rolling. Moreover, dislocations in the rolled surface for BNII are less than CPII, resulting in a decrease of corrosion	[33]

(*continued on next page*)

Table 1 (*continued*)

Grain size, D (μm)	Process	Material	Solution	D decreases ➔ CR ?	How to change D	The mechanism	Ref.
12.3–0.35	High Ratio Diff. Speed Rolling (HRDSR)	Pure Ti	0.5 M H2SO4 solution	Decreases	High Ratio Differential Speed Rolling (HRDSR)	Due to grain refinement by HRDSR and making UFG Ti, corrosion resistance has been enhanced. After annealing, corrosion resistance of UFG Ti was further increased which was attributed to the dislocation density and residual stress reduction after annealing	[34]
200–0.5	ECAP	Pure Al	0.01 mol/L sodium sulfate (Na2SO4) water solution containing 0.01% Cl-.	Decreases	ECAP (Room Temp.)	A large fraction of non-equilibrium grain boundaries and high residual stress in UFG industrially pure Al results in more nucleation sites for the formation of the passive layer and hence denser oxide film than CG (Coarse Grains) will form	[35]
250–35	Heat Treatment (from As Cast)	AZ31B	3.5 wt.% NaCl	Decreases (500–300 °C) due to grain refinement Increases (300–200 °C) due to increase in twins	Temp. change (200–500 °C)	A higher dislocation density and twins probably result in higher anodic reaction. Grain boundaries act as corrosion barriers. More grain boundaries result in slow down the corrosion rate. In the sample heat-treated at 300 °C, the high density of twins has been eliminated, but the grain size did not change significantly, resulting in a relatively lower corrosion rate.	[36]
70–0.65	FSP	Mg-Y-RE	3.5 wt.% NaCl	Decreases	HT for grain enlargement, and FSP for refinement	In the UFG sample, the high fraction of grain boundaries probably reduces corrosion rate in two ways: (1) accelerating the passivation phenomena and (2) reducing the intensity of galvanic couple between grain interior and grain boundary, leading to more uniform degradation and lower corrosion rates.	[37]
11–1.4	Hot extrusion	AZ31B	0.1 M NaCl	Decreases	Process time	Grain refinement may relieve the stress on the surface film, due to mismatch between corrosion products (MgO) and underlying Mg metal, by producing vacancies via grain boundaries, thus increase the passivity of the surface film. This would improve the stability of the surface film of UFG Mg alloy.	[38]
–	ECAP	AZ91D	3.5 wt.% NaCl	Increases	Num. of passes	The corrosion rate of ECAPed AZ91D alloy was increased, due to severely deformed UFG matrix and the refined β-phase. More crystalline defects cause the matrix to become more corrosion activated and increase the corrosion rate of the α-phase matrix. When the β-phase changes from the net-like shape into isolated shape and fine particles distribute uniformly, its barrier functionality to the corrosion progress will be eliminated. The interaction of two factors also causes the corrosion behavior change from pitting corrosion into serious uniform corrosion of AZ91D alloy.	[39]

(*continued on next page*)

Table 1 (*continued*)

Grain size, D (μm)	Process	Material	Solution	D decreases ➔ CR ?	How to change D	The mechanism	Ref.
80 (Cast)−4.6–7.1 (Extrusion)	Extrusion	AZ80	3.5 wt.% NaCl Saturated with Mg(OH)2	Decrease and increase	Extrusion at Different Temps. (250, 300 and 350 °C)	The corrosion rate of the extruded alloy was more than cast alloy, due to the breakdown of the net-like β-phase. An increase in the temperature from 250 to 300 °C (in a trend that grain size increases) the corrosion rate was increased, due to the increase of dislocation density. However, this concept does not seem to be valid, because the dislocation density like., grain boundary length decreases with the increase of the deformation temperature. The dislocation density was measured using the TEM which is a local analysis and it may not be extrapolated to the whole sample. The corrosion rate slightly decreased from 300 to 350 °C, but no specific reason was mentioned.	[40]
	ECAPed	1050 Al	0.1 M sodium sulfate (Na_2SO_4) solution	Decreases	Number of passes	The size of the Si-containing phases decreased with increasing ECAP pass numbers (N). In addition, to increasing N, the second phase was spread more uniformly. The ECAPed alloy showed a rather stable oxide layer. The pit forming mechanism of the ECAPed sample was related to the galvanic corrosion between the Al matrix (anode) and Si-containing phase or a mixed oxide containing Si (cathode). Hence, using the ECAP technique the size of the Si-containing phases as well as their total area was decreased. Thus, the pitting resistance was increased with increasing N.	[41]

- Enhancement of a more uniform and coherent passivation layer by grain refinement.
- More grain boundaries act as more barriers against preferred crystallographic pitting (PCP)
- Enhancement the basal plane intensity (as a side effect of grain refinement depending on the deformation processes)

It is clear from the reports that the type of alloy, distribution of second phases, processing routes for changing the grain size, and electrolyte type result in different trends. In order to understand the real effect of the grain size on the corrosion behavior, we have classified these studies into two major groups including pure metals and alloys.

Fig. 1 shows the results of electrochemical study including open circuit potential (OCP) and electrochemical impedance spectroscopy (EIS) of pure Mg extruded at 260 °C followed by multi -directional forging (MDF) at various temperatures (220, 260, 300 and 340 °C) in 3.5 wt.% NaCl saturated with $Mg(OH)_2$ solution. The details of this experiment have been mentioned elsewhere [19]. The OCP values from the initial 0.5 h (Fig. 1(a)) and after 24 h (Fig. 1(b)) shows that corrosion products that form on the surface of all the samples gradually shifted the surface potential to the nobler direction. The potential has a direct relationship with the grain size. Since grain boundaries have a lower potential than the matrix, OCP shifts to lower values. The EIS Nyquist plots of the 0.5 h immersed samples depict that MDF at lower temperatures improved the corrosion resistance of pure Mg. The increase in diameter of the semi-circle of the MDF220 sample clearly shows that material with smaller grain size has more ability to acquire the passivity behavior, due to the more coherent and stable passive layer formed on the exposed surface of the metal with more grain boundaries. In fact, grain boundaries, by providing more dislocations, compensate the mismatch of the hydroxide/oxide layer with the base metal [20–23]. Changing the grain size by changing process conditions such as temperature, number of process passes, the direction of applying deformation, and casting cooling rate will also change the second phase distribution and matrix concentration, so these effects also need to be considered in corrosion behavior of alloys.

Fig. 2 depicts the corrosion rate vs grain size of pure Mg obtained from different studies. It seems that even in the pure Mg, the single trend in corrosion rate vs grain size was not noticed. While in some cases, corrosion rate increases with increasing the grain size, in others it decreases. As a matter of fact, grain boundaries are the high energy sites and so, corrosion initiates from these sites. With an assumption of no defect in the material, grain boundaries should increase the corrosion rate. That is why a single crystal material with the packed orientation like basal plane exposed to the corrosion has a very low corrosion rate (~0.5 mm/y in simulated body fluid (SBF) for 1d immersion) [8]. But adding grain boundaries and decreasing the grain size, increases the corrosion rate by localizing the corrosion and breaking down the surface layer. However, in the majority of the cases, the corrosion rate has been decreased by decreasing the grain size.

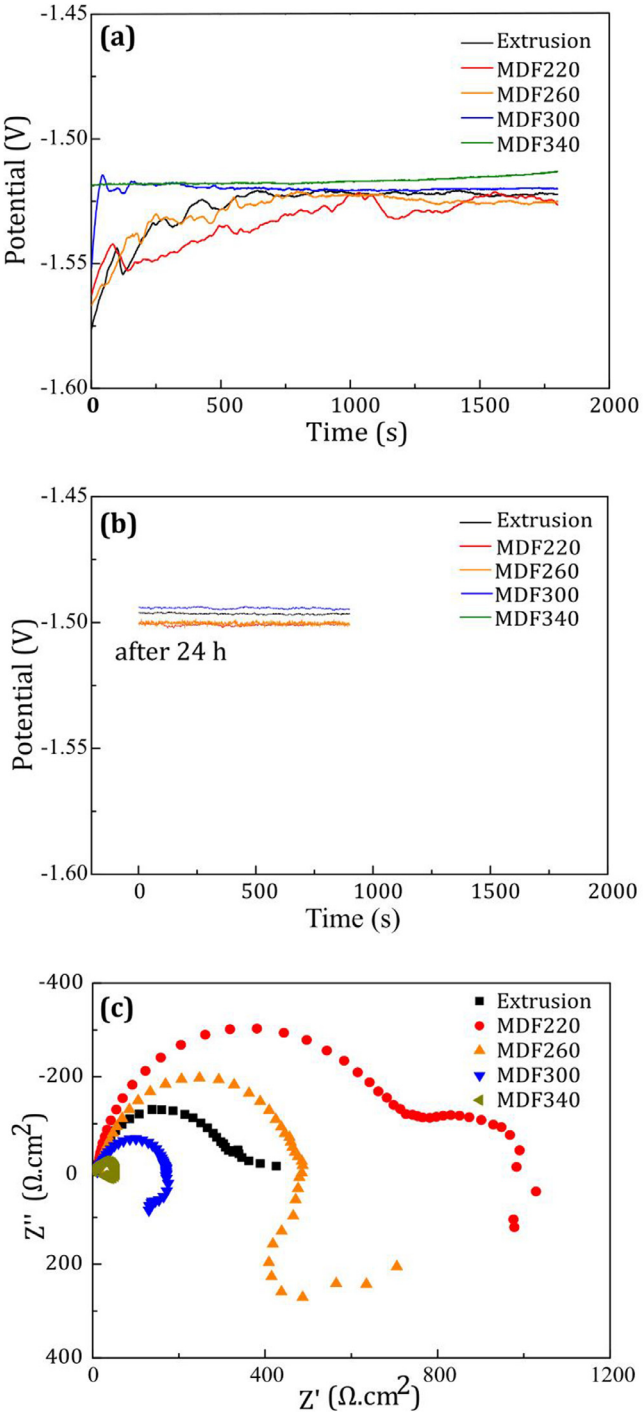

Fig. 1. The electrochemical study results of extruded and MDF pure Mg (a) OCP within 0.5 h immersion, (b) OCP after 24 h and (c) EIS after 0.5 h immersion [19].

So it can be concluded that in the case of single grains like single crystals or bi-crystals, corrosion rate increases with increasing the grain size, while in very fine grains (maybe less than 50 μm in) corrosion rate decreases by decreasing the grain size. However, the possibility of passivation due to the

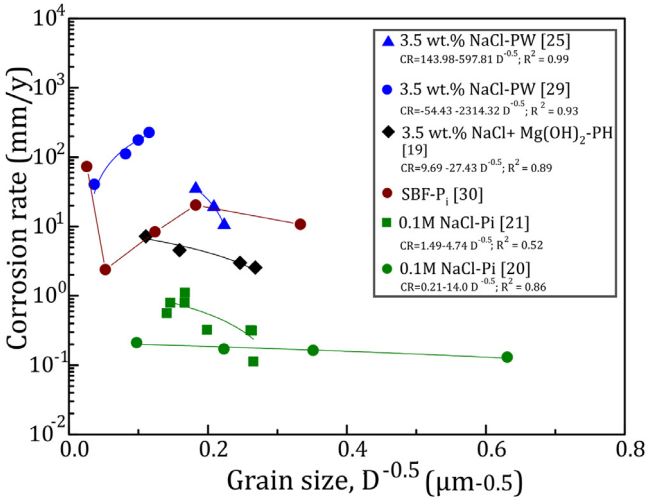

Fig. 2. Effect of grain size on the corrosion rate of pure Mg [19–21,25,29,30] (P_i, P_w and P_H are corrosion rate measured by polarization, weight loss and hydrogen evolution methods, respectively).

solution property should be considered. Less aggressive solutions like 0.1 M NaCl will probably increase the range of passivation, so the grain size tolerance to provide the passivating layer increases (Fig. 3).

To formulate the effect of grain size on the corrosion rate we may use the Hall-Petch type equation that was proposed by Ralston et al. [21]. The corrosion rate is related to the grain boundary length (GBL) and GBL is linearly related to $D^{-0.5}$, where D is the grain size. Therefore the corrosion rate (CR) can be written as follows:

$$CR = a + b \times D^{-0.5} \tag{8}$$

Where a, and b are the fitting constants related to other parameters which will be discussed later. Since grain size effect should be applied just on the matrix, a surface fraction of matrix, $f_{A,m}$ (=1- $\Sigma f_{A,i}$), was multiplied by the term D. Therefore the equation could be changed as:

$$CR = a + b \times f_{A,m} \times D^{-0.5} \tag{9}$$

As explained, the grain size may have effects in two different ways [20, 21,35,42], so the grain size-related corrosion can be written as:

(1) $-b_1 \times f_{A,m} \times D^{-0.5}$ for small grains or solutions providing passivation. "-" depicts that corrosion rate increases with increasing grain size [20, 21,43,44]

(2) $+b_2 \times f_{A,m} \times D^{-0.5}$ for very large grains including single- or bi-crystals or in solutions where passivation is not possible. "+" shows that the corrosion rate decreases with increasing grain size [30,35,42].

One of the most effective ways to achieve ultra-fine grains are using severe plastic deformation, where not only yield strength can be effectively improved, but also, the corrosion rate can be decreased [45]. Several SPD techniques such as equal channel angular pressing/extrusion (ECAP/ECAE) [46–51], high ration differential speed rolling (HRDSR) [52–54], accumulative roll bonding (ARB) [55–58], accumulative back extrusion (ABE) [59–63], three roll planetary milling or screw rolling (SR) [64–66], friction stir welding (FSW) [67–70], high pressure torsion [71–74] and multi-directional forging (MDF) [75–84] have been reported. Using these techniques or any other process like powder metallurgy, it is possible to achieve UFG or even nano-grains.

1.1.3. Second phase (phase fraction and volta-potential)

One of the most important factors influencing the corrosion behavior of alloys is the galvanic corrosion which can be formed between the intermetallic phases and matrix. The potential difference between the intermetallic phase and matrix is the driving force for the electrons to move from anode to cathode and form the galvanic cells. The anodic second phase degrades in contact with the nobler matrix in a galvanic cell, whereas the matrix degrades when the second phase is nobler than the matrix. Fig. 4 shows the effect of volta-potential difference and intermetallic phase fraction on the corrosion propagation at the surface where an increase in the Volta-potential difference between intermetallic phase and the matrix accelerates the matrix degradation and so the corrosion rate increases. An increase in the fraction of the second phase also provide more active galvanic cells and so the affected area by corrosion rate will linearly increase. The corrosion rate related to the micro-galvanic cells (intermetallic) can be defined by considering the volta-potential difference, showing the kinetic of reaction and area fraction of the phase showing the available sites.

Atrens et al. [17,18,85–88] have done several studies on binary alloys and investigated the effect of alloying elements on the corrosion rate and corrosion behavior of Mg alloys. However, a potential distribution study besides their alloys will probably open a new window towards the corrosion rate prediction of Mg alloys. The potential difference between the intermetallic phases and matrix can be obtained through direct measurement of potential of each phase, using OCP [89], SKPFM [90,91], and/or first principle calculation through measuring the surface potential and work function [4].

Table 3. shows the Volta-potential difference of various intermetallics relative to the matrix, obtained from the literature. Since Mg is one of the most active elements in the series of standard electrode potential and its work function (WF) is less than the majority of alloying elements, most of the intermetallic phases act as cathode for the Mg-rich matrix. But if the matrix potential increases or alloying elements with smaller work function than Mg (WF = 3.66) such as Ca (WF = 2.8), Ce (WF = 3.1), Nd (WF = 3.2), or Y (WF = 3.1) is used, the anodic intermetallic phases can be formed. As it can be seen in the following image (Fig. 5), Mg-Ce, Mg-Nd-Y, and Mg_2Ca phases showed the anodic behavior relative to the matrix. But the rest of the intermetallics showed cathodic behavior.

To understand the mechanism of corrosion propagation on the surface of materials with the anodic or cathodic second phase, the corroded surface of two materials after 0.5 h

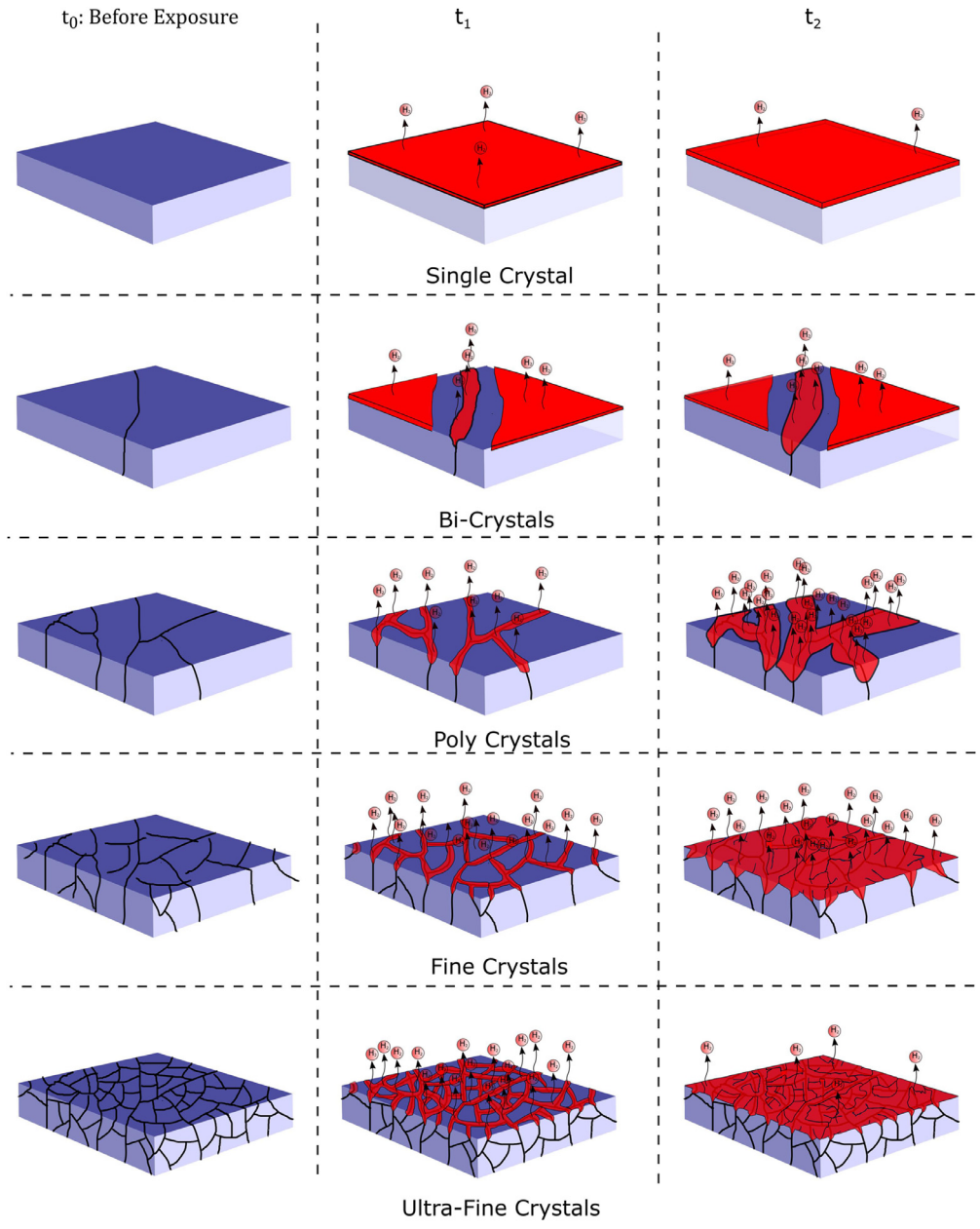

Fig. 3. Schematic representation of the effect of grain size refinement on corrosion propagation.

immersion in 3.5 NaCl solution saturated with $Mg(OH)_2$ were compared. Fig. 5(a-c) shows the Volta-potential distribution of the XM11 alloy with anodic Mg_2Ca phase, Mg_2Ca phase distribution, and SEM image of this alloy immersed for 0.5 h, after removing the corrosion products to visualize the remaining material. As confirmed from the SKPFM results, the Mg_2Ca is an anodic phase, thus dissolved during the corrosion process. A kind of filiform corrosion has also been propagated on the matrix which shows not only the second phase needs to be considered, but also matrix properties affect the corrosion behavior. This phase protected the matrix undergoing severe corrosion, but after its dissolution, the corrosion propagated on the surface as filiform corrosion and dissolved the matrix. Fig. 5(d) shows the schematic corrosion mechanism of the alloy containing the anodic phase. Here, the corrosion initiates through the dissolution of Mg_2Ca and the matrix will be protected until Mg_2Ca is dissolved. After the dissolution of the Mg_2Ca, the matrix would not be protected and corrosion propagates on the surface, preferentially by dissolving the grain boundaries and then grains, until the surface is fully covered by the corrosion products. This kind of corrosion may form as filiform corrosion, later the passivation by corrosion products reduces the overall corrosion rate. This phenomenon could be the reason for the high corrosion rate during the initial stages of immersion. Fig. 5(e) is the volta-potential distribution of the ZAXM4211 alloy showing that intermetallic phases are cathodic with respect to the matrix. The SKPFM result confirms that both the second phases that are present on the surface are cathodic. The phase distribution on the surface of this material is shown in Fig. 5(f). Here, there are

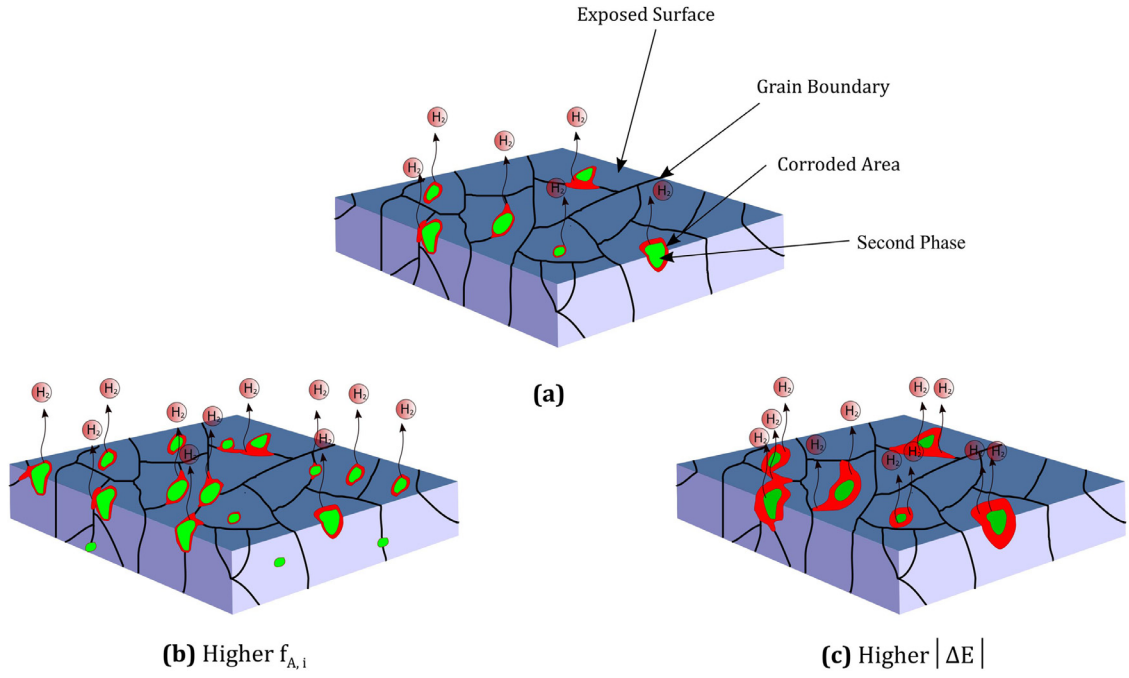

Fig. 4. Effect of Volta-potential difference and second phase fraction on corrosion rate: (a) Degradation of the matrix adjacent to the second phase for a given material, (b) more degradation due to higher Volta-potential difference and (c) more degradation compared to (a) due to higher area fraction of secondary phases.

Table 2
Volta-potential values of different phases observed in Fig. 5 compared with pure Mg and Pt.

Material	E_α (mV)	Intermetallic	E_i (mV)	$\Delta E = E_\alpha$-E_i (mV)
Pt	210.26 ± 10	–	–	–
Pure Mg	1704.40 ± 15	–	–	–
XM11	1806.28 ± 27		1932 ± 13	−126
ZAXM4211	1298.30 ± 44	(Mg, Al)$_2$Ca+MgZn	906 ± 29	392
		Al_8Mn_5	991 ± 35	307

two phases including Al_8Mn_5 which is stable in high temperatures and has a sharp morphology and (Mg,Al)$_2$Ca+MgZn phase which forms during solidification between the dendrites and has an elongated shape. Fig. 5(g) shows the SEM image of the immersed ZAXM4211 alloy (after removing corrosion product) and clearly indicating the matrix corrosion adjacent to the second phase. Fig. 5(h) shows the schematic corrosion mechanism of the alloy containing the cathodic second phase. Corrosion initiates by the dissolution of the matrix adjacent to the second phase, the corrosion propagates along the matrix as filiform corrosion by the dissolution of the weaker sites, i.e. grain boundaries, while second phases remain undissolved. Therefore, based on the stability and compactness of the formed surface layer, the corrosion rate decreases.

The Volta-potential values of the XM11 and ZAXM4211 alloys in addition to pure Mg and Pt have been presented in Table 2. The matrix potential has been shifted towards the more noble direction where the surface potential of pure Mg and ZAXM4211 alloy is 1704.4 mV and 1298.3, respectively. The surface potential of pure Pt also was measured and it was found that the potential of Pt which is one of the noblest materials is 210 mV.

Hurley et al. [3] reviewed the Volta-potential difference of various secondary phases. Here, using their reviewed and reported data, Table 3 has been presented adding other phases and making average from the available data of particular phases.

Hence, the second phase effect was divided into two mechanisms including anodic ($c_a \times \Sigma(f_{A,a} \times |\Delta E_a|)$) and cathodic ($c_c \times \Sigma(f_{A,c} \times |\Delta E_c|)$) second phases and the corrosion rate related to the second phases were defined as:

$$CR_i = A + \left[c_a \times \Sigma\left(f_{A,a} \times |\Delta E_a|\right]\right] + \left[c_c \times \Sigma\left(f_{A,c} \times |\Delta E_c|\right]\right] \quad (10)$$

Where A, c_a, c_c, $f_{A,a}$, $f_{A,c}$, $|\Delta E_a|$ and $|\Delta E_c|$ are the corrosion rate of the material without any second phase, contribution of anodic second phases, contribution of cathodic second phases, area fraction of anodic phase, area fraction of cathodic phase, absolute value of the Volta-potential difference of matrix relative to the anodic second phase and volta-potential difference of matrix relative to the cathodic second phase, respectively.

Since an increase in ΔE regardless of cathodic or anodic phase increases the corrosion rate, we can use $|\Delta E|$ and simplify this term as $[c \times \Sigma(f_{A,i} \times |\Delta E|)]$ where c and $f_{A,i}$ are the contributions and area fraction of the second phases, respectively.

Fig. 6 presents the surface analysis of the ZAXM4211 alloy produced in various conditions. The Volta-potential

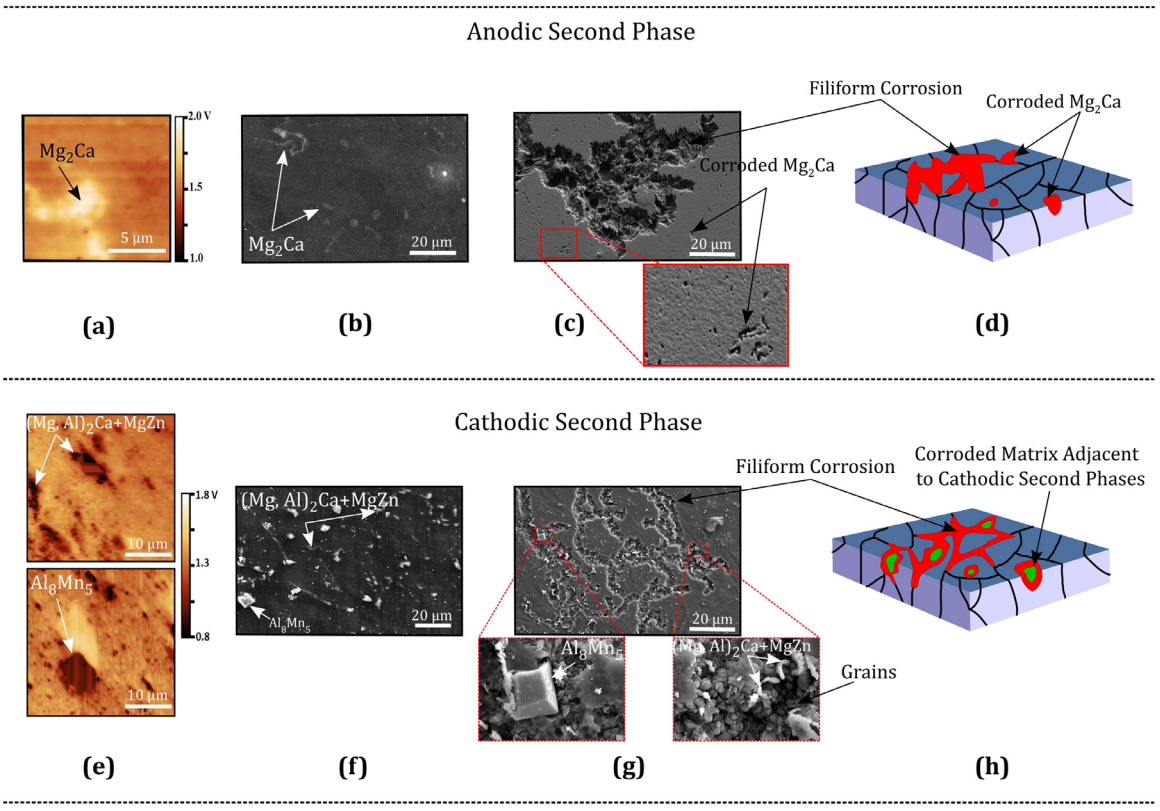

Fig. 5. Mechanisms of corrosion propagation on materials with anodic or cathodic second phases: (a) Volta-potential distribution of a Ca-containing Mg alloy (XM11 alloy) with anodic intermetallic of Mg_2Ca, (b) distribution of the secondary phase on XM11 alloy before immersion, (c) SEM image after 0.5 h immersion in 3.5 NaCl saturated with $Mg(OH)_2$ solution (after removing corrosion product) showing the degraded second phases, (d) corrosion propagation mechanism of the Ca-containing alloy, (e) volta-potential distribution of a Mn, Al, Ca, and Zn-containing Mg alloy (ZAXM4211 alloy) with cathodic Al_8Mn_5 and (Mg, Al)$_2$Ca+MgZn phases, (f) distribution of the secondary phases on the ZAXM4211 alloy before immersion, (g) SEM image of the immersed ZAXM4211 alloy (after removing corrosion product) showing the corroded matrix adjacent to second phases and (h) corrosion propagation mechanism of the alloy containing the cathodic phases [19,92].

Table 3
Volta-potential difference of different intermetallics with matrix for magnesium alloys.

Phase	Pot. Diff.	Alloy	Ref.	Phase	Pot. Diff.	Alloy	Ref.
Al-Ca (Sn,Sr)	62	Mg-Al-Ca	[93]	Zr-Zn-Fe	180	ZE41	[94]
Al-Mn	303±66	–	[3, 40, 95–99]	Y-Mg-Nd-RE(La,Ce,Gd)-Si	50	WE54-T6	[94]
Al-Gd	90	AM50Gd	[100]	Zr-Mg-Fe-Ni	250	WE54-T6	[94]
Al-Mn-Gd	206±40	–	[98, 100]	Al-Mn-Nd	250	AZ91-Nd	[101]
Al-Mn-Nd	115	AM50Nd	[3]	Al-Nd	140	AZ91-Nd	[101]
Al-Nd	30	–	[95, 102]	Mg-Nd-Y	−35	EW75	[103]
Mg-Al	78±715	–	[40, 94, 95, 98, 104, 105]	Al_2Y	320	EW75	[103]
Mg-Al-Ce	11	AMCe	[105]	(Mg, Al)$_2$Ca	250	AZCW6110	[106]
Mg-Al-La	8	AMLa	[105]	(Al_8Mn_5)Y	450	AZCW6110	[106]
Mg-Ce	−85	Mg-2Ce	[3]	Mg_2Ca	−130	XM11	[19, 107]
Mg-La	111	Mg-1La	[3]	Ca-Mg-Zn	350	ZXM411	[19]
Mg-Nd	150	Mg-2.6Nd	[108]	Al-Mn	190	ZAXM4411	[19]
Mg-Nd-Y	15	WE43-T6	[94]	Φ (Zn-Mg-Al-Ca)	230	ZAXM4411	[19]
Mg-Si	97	AZ80	[109]	(Mg, Al)$_2$Ca	397	ZAXM4211	[19]
Mg-Si-Ca	408	ZSM651+0.8Ca	[3]	Al-Mn	310	ZAXM4211	[19]
Mg-Zn	551	ZSM651+0.8Ca	[3, 104]	Φ (Zn-Mg-Al-Ca)	388	ZAXM4221	[19]
Mg-Zn-RE (La,Ce,Gd)	100	ZE41	[3, 94]	(Mg, Sn)$_2$Ca	254	TXM911	[19]
Mg-Zn-RE (La,Ce)	100	ZE41	[94]	Mg-Sn-Zn-Ca	200	TZXM4411	[19]
Mg-Si	428	ZSM651+0.8Ca	[104]	Φ (Zn-Mg-Al-Ca)	388	ZAXM4221	[19]
Y-Mg-Nd-RE(La,Ce,Gd)-Si	50	WE43-T6	[94]	(Mg, Al)$_2$Ca	533	AXM211	[19]
Zr-Mg-Fe-Si	180	WE43-T6	[94]	MgZn	510	ZM41	[19]

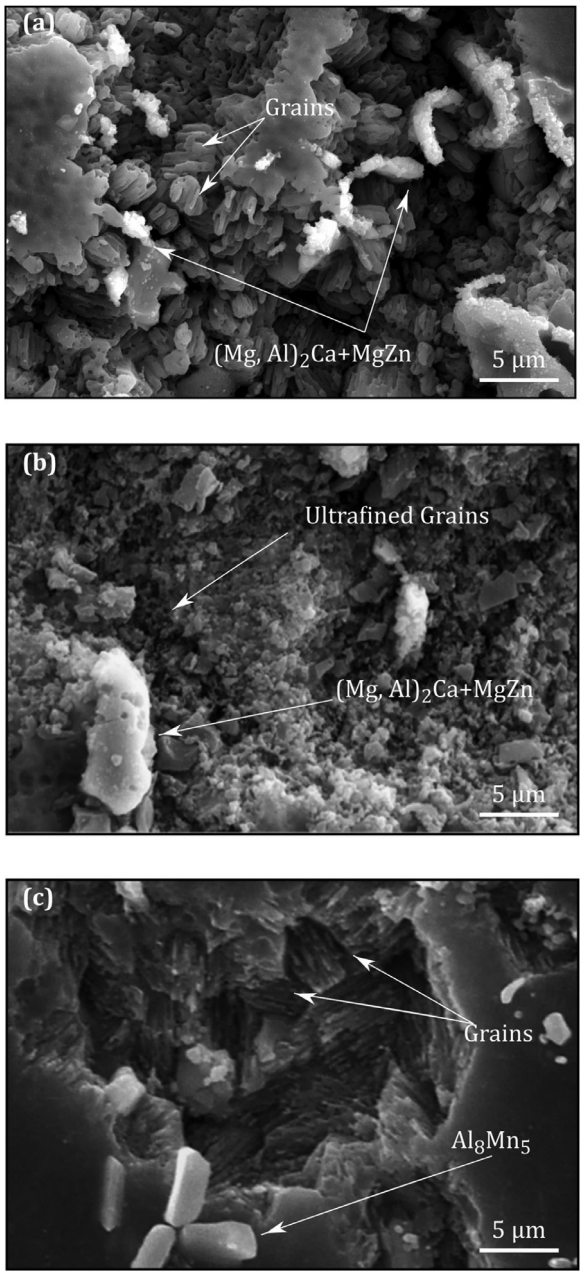

Fig. 6. The SEM image of the 0.5 h immersed ZAXM4211 alloy: (a) extruded, (b) MDF180 and (c) MDF300.

distribution presented in Fig. 5 and Table 2 showed the intermetallic phases in this alloy are cathodic. This fact was proved by SEM images where, after immersion and removing corrosion products, the second phases are intact. From Fig. 6, it is clear that the grain boundaries have been corroded and so the effect of grain boundaries as well as the second phase needs to be considered.

1.1.4. Corrosion rate formulation

Total corrosion rate equation based upon the microstructural parameters can be written as:

$$CR = a_C \times \left(\sum f_{or} \times CR_{or}\right) - CR_{P,C} - b_1 \times f_{A,m} \times D^{-0.5} + b_2 \times f_{A,m} \times D^{-0.5} + c \times \Sigma\left(f_{A,i} \times |\Delta E|\right) \quad (11)$$

Where the first term ($a_C \times (\Sigma f_{or} \times CR_{or})$) is the corrosion rate of grains related to the crystallographic texture (orientation), change in surface energy by the addition of alloying elements to pure metal or changing the dislocation density of grains. $CR_{P,C}$ is the passivation effect which can be changed by the alloy composition change. In present study, the texture effect has been assumed to be constant, due to the randomized texture. However, when the basal planes fraction changes, the area fraction of each orientation should be considered to analyze the corrosion results. Therefore, the above-mentioned Eq. (11) can be re-written as follows;

$$CR = \left[CR_{T,C} - CR_{P,C}\right] - b_1 \times f_{A,m} \times D^{-0.5} + b_2 \times f_{A,m} \times D^{-0.5} + c \times \Sigma(f_{A,i} \times |\Delta E|) \quad (12)$$

Considering $CR_{T,C} - CR_{P,C} = CR_0$;

$$CR = CR_0 - b_1 \times f_{A,m} \times D^{-0.5} + b_2 \times f_{A,m} \times D^{-0.5} + c \times \Sigma\left(f_{A,i} \times |\Delta E|\right) \quad (13)$$

We may further consider b_2-$b_1 = b$ *to* combine the intrinsic and extrinsic effects of grain size and rewrite the Eq. (13) as Eq. (14) which is proposed as a final equation:

$$CR = CR_0 + b \times f_{A,m} \times D^{-0.5} + c \times \Sigma\left(f_{A,i} \times |\Delta E|\right) \quad (14)$$

CR_0 is related to the matrix surface energy (changing by the concentration of the solute atoms and density of dislocations) and the distribution of different orientations. The contribution of grain size in the corrosion rate is denoted as "b", which is related to the corrosive solution. It should be kept in mind that this value is positive for very large grains and negative for fine grains (the critical point is related to the solution). The contribution of the second phase, 'c', could be changed by the type of secondary phases (anodic, cathodic), and corrosive solution.

The corrosion rate is intensely affected by the solution type [110–114]. In fact, the solution type will change all CR_0, b and c parameters. By changing the concentration of NaCl in the aqueous solution, Liu et al. [110] found that the corrosion rate is directly related to Cl^- ion concentration. They mentioned that the higher concentration of NaCl results in the breakdown of the surface film, so CR_0 needs to be decreased hereby increasing the NaCl concentration. However, once the surface film is broken down, the second phase and grain boundaries will be activated because of solution exposure. Hence, their contribution (b and c parameters) should also be changed.

It can finally be mentioned that, considering the effect of alloy composition, grain size, and the galvanic cell can predict the corrosion rate with a good agreement as shown in Fig. 7. The related values and conditions of the corrosion rate measurement methods have been given in Table 4.

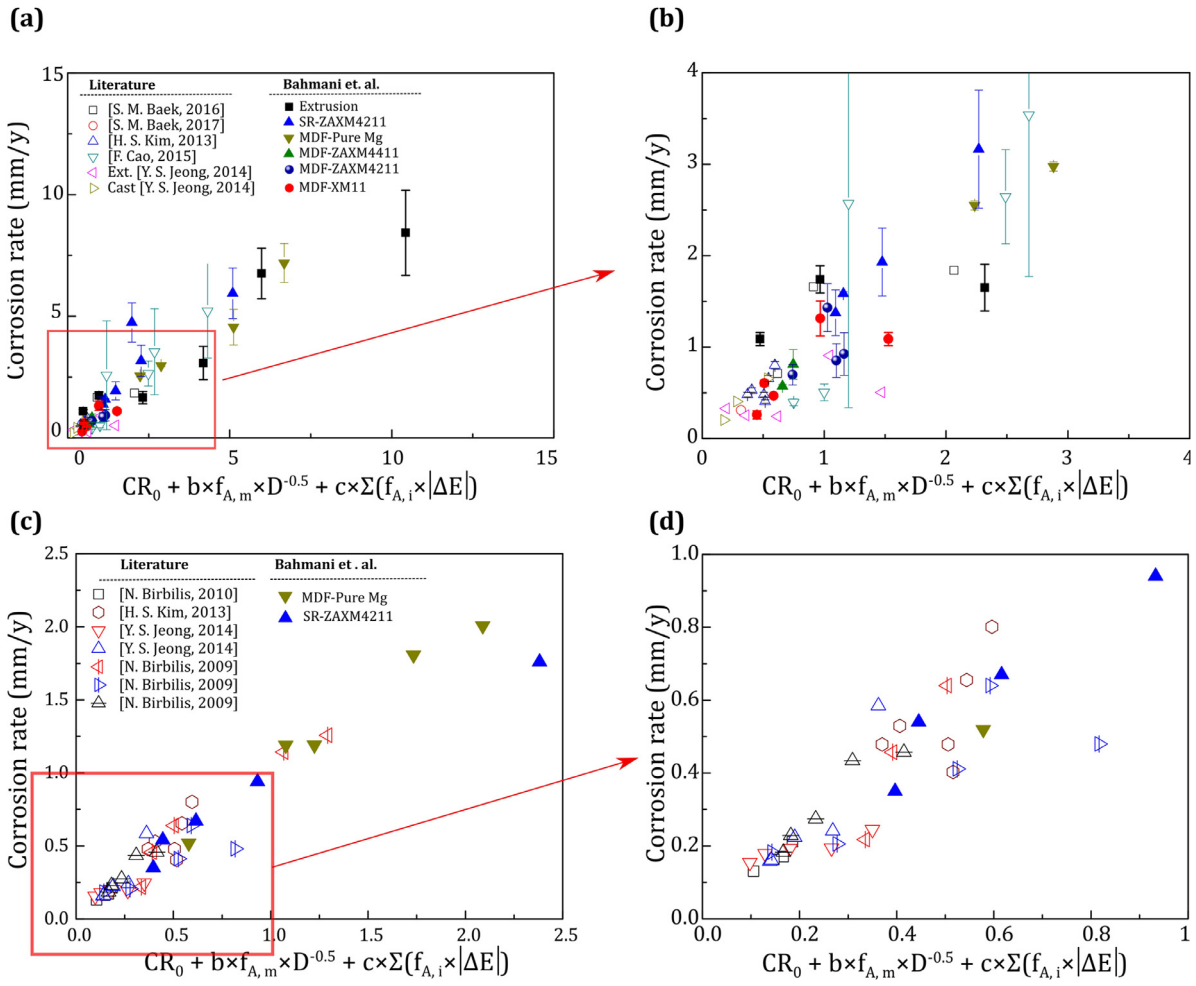

Fig. 7. (a) The experimental corrosion rate versus corrosion rate obtained by the proposed model. (a) and (b) the corrosion rate measured by hydrogen evolution or weight loss methods and (c) and (d) the corrosion rate measured by the electrochemical study.

In case of data for which the fraction of phases has not been directly mentioned in the paper, the phase fraction was measured by image analysis from the available data [17,86] or JMatPro commercial software [115]. If the volta-potential has not been measured, the available volta-potential difference values were used in Table 3. To avoid a messy graph, the graphs were separated to those data related to the hydrogen evolution or weigh loss in Fig. 7(a) and (b) and (c) and (d) are related to the electrochemical study. Since the electrochemical corrosion rate in Mg alloys is less than that of obtained by hydrogen evolution and weight loss [85, 116], lower CR_0, b and c values need to be used for the proposed model. For example, as can be seen in Table 4, CR_0, b and c values used for the corrosion rate calculation of rolled and annealed AZ61, reported by Kim et al. [44] are 0.5, −0.25 and 0.01 respectively for the weight loss rate, while the same parameters have the values of 0.2, −0.15 and 0.01 respectively when CR was calculated from the electrochemical polarization test. Moreover, various solutions have different intensities in corroding the exposed alloy. For instance, increasing the Cl^- ions by adding more NaCl, increases the corrosion rate because of accelerating the anodic reaction and increasing the Mg dissolution. So in this case of solutions with a higher tendency for degradation, higher values are required for the balancing parameters.

Another point which is considered is the second phases that are anodic relative to the matrix have different b value comparing to the cathodic phases. For example, b value in the study of Birbilis et al. [115] for the Mg-Ce alloys containing Mg-Ce phase which is anodic against Mg matrix [3] is 3 times higher than that of the Mg-La and Mg-Nd alloys. Same results were achieved by the authors where b value in the case of an alloy containing Mg_2Ca phase which is anode was higher than that of other cathodic phases (please see Tables 3 and 4). This is due to a different mechanism of corrosion for the alloy containing cathodic and anodic phases, as it has been seen in Fig. 5. However, the agreement of results between calculation and actual corrosion rates of all Mg alloys in the graph of Fig. 7 shows that both types of alloys can be used in this equation just by different balancing values.

Table 4
The conditions of the various studies in the Fig. 7. Solutions are: S1: 3.5 wt.% NaCl with Saturated $Mg(OH)_2$, S2: 3.5 wt.% NaCl, S3: Hank, S4: 0.1 M NaCl. Corrosion rate measuring methods are: P_H: Hydrogen evolution, P_W: Weight loss and P_i: electrochemical polarization.

Reference	CR0	b	c	Solution	Measurement method	Alloy	Process
F. Cao, 2015 [17, 117]	1.0	−5.0	0.3	S1	P_H	HP Mg, 1.0 wt.%Mn 0.3 wt.% Ca, 6.0 wt.%Al 5.0 wt.% Zn, 0.7 wt.% Nd	Cast
S. M. Baek, 2016 [118]	1.5	−5.0	0.2	S2	P_W	AZ61-xCa	Extrusion
S. M. Baek, 2017 [106]	0.5	−5.0	0.2	S2	P_W	AZ61-0.6Ca-0.3Y	Extrusion
Y. S. Jeong, 2014 [119]	0.2	−0.2	0.2	S3	P_H	Mg-xCa	Cast and extrusion
H. S. Kim, 2013 [44]	0.5	−0.25	0.01	S4	P_W	AZ61	Rolling and annealing
A. Bahmani [92]	0.5	−5.0	0.2	S1	P_H	ZAX421	MDF
A. Bahmani [120]	0.5	−7.0	0.2	S1	P_H	ZAX421	SR
A. Bahmani [19, 107, 121]	0.5	−5.0	0.2	S1	P_H	Alloys	Extrusion
A. Bahmani [19]	9.8	−28.1	—	S1	P_H	Pure Mg	MDF
A. Bahmani [19]	1.5	−5.0	0.2	S1	P_H	XM11	MDF
A. Bahmani [92]	0.5	−5.0	0.2	S1	P_H	ZAX441	MDF
Y. S. Jeong, 2014 [119]	0.2	−0.2	0.2	S3	P_H	Mg-xCa	Cast and extrusion
H. S. Kim, 2013 [44]	0.5	−0.25	0.01	S4	P_W	AZ61	Rolling and annealing
N. Birbilis, 2010 [20]	0.2	−0.15	–	S4	P_i	Pure Mg	ECAP
N. Birbilis, 2009 [115]	0.2	−0.15	0.06	S4	P_i	Mg-xCe	Cast
N. Birbilis, 2009 [115]	0.2	−0.15	0.02	S4	P_i	Mg-xLa Mg-xNd	Cast
H. S. Kim, 2013 [44]	0.2	−0.15	0.01	S4	P_i	AZ61	Rolling and annealing
Y. S. Jeong, 2014 [119]	0.2	−0.2	0.1	S3	P_i	Mg-xCa	Cast, Extrusion
A. Bahmani [19]	2.8	−6.4	—	S1	P_i	Pure Mg	Ext and MDF
A. Bahmani [120]	0.2	−4.0	0.1	S1	P_i	ZAXM4211	SR
A. Bahmani [92]	0.2	−2.6	0.2	S1	P_i	ZAXM4211	MDF

3. Conclusions

An attempt was made to model the corrosion rate of Mg alloys based on the microstructural parameters. This model can be applicable for all the alloys; however, the main focus of this paper was on various Mg alloys. Based upon the explained results, the following conclusions were drawn:

Corrosion rate can be calculated by considering the role of composition, grain size and second phases and other affecting parameters can also be applied in these terms.

- The alloy composition influences the corrosion rate through several ways such as changing the surface potential of different orientations, changing the passivating layer properties and producing second phases. The second phase was formulated as an independent term here, while the passivation and surface potential can be considered as a term named as CR_0. The other parameter which can influence this term is the texture, where the basal texture has been proven to be more corrosion-resistant than the others.
- By considering the effect of grain boundaries, grain size may affect two different ways including acceleration of the corrosion in non-passivating solutions or in very large grain materials (such as single crystal) or providing more coherent and uniform passive film and protecting the substrate from further corrosion in fine and ultrafine grains and also in passivating solutions.
- The effect of second phases was included by considering their potential difference with matrix and area fraction.
- Regarding the above-mentioned parameters, an experimental equation was proposed and explained by all the parameters where it has a good match with our results and available literature.
- Moreover, a material which has a very low corrosion rate was found in our work where its corrosion rate is much less than high purity Mg.

Acknowledgment

This work was supported by the National Research Foundation grant (2015R1A2A1A01006795) funded by the Ministry of Science and ICT of Korea through the Research Institute of Advanced Materials.

References

[1] M. Esmaily, J.E. Svensson, S. Fajardo, N. Birbilis, G.S. Frankel, S. Virtanen, R. Arrabal, S. Thomas, L.G. Johansson, Fundamentals and advances in magnesium alloy corrosion, Prog. Mater Sci. 89 (2017) 92–193.
[2] G.B. Hamu, D. Eliezer, L. Wagner, The relation between severe plastic deformation microstructure and corrosion behavior of AZ31 magnesium alloy, J. Alloys Compd. 468 (1–2) (2009) 222–229.
[3] M.F. Hurley, C.M. Efaw, P.H. Davis, J.R. Croteau, E. Graugnard, N. Birbilis, Volta potentials measured by scanning kelvin probe force microscopy as relevant to corrosion of magnesium alloys, Corrosion 71 (2) (2015) 160–170.
[4] P.R. Cha, H.S. Han, G.F. Yang, Y.C. Kim, K.H. Hong, S.C. Lee, J.Y. Jung, J.P. Ahn, Y.Y. Kim, S.Y. Cho, J.Y. Byun, K.S. Lee, S.J. Yang, H.K. Seok, Biodegradability engineering of biodegradable Mg alloys: tailoring the electrochemical properties and microstructure of constituent phases, Sci. Rep. 3 (2013) 2367.
[5] R. Xin, Y. Luo, A. Zuo, J. Gao, Q. Liu, Texture effect on corrosion behavior of AZ31 Mg alloy in simulated physiological environment, Mater. Lett. 72 (2012) 1–4.

[6] K.S. Shin, M.Z. Bian, N.D. Nam, Effects of crystallographic orientation on corrosion behavior of magnesium single crystals, JOM 64 (6) (2012) 664–670.
[7] G.-L. Song, The effect of texture on the corrosion behavior of AZ31 Mg alloy, JOM 64 (6) (2012) 671–679.
[8] K. Hagihara, M. Okubo, M. Yamasaki, T. Nakano, Crystal-orientation-dependent corrosion behaviour of single crystals of a pure Mg and Mg-Al and Mg-Cu solid solutions, Corros. Sci. 109 (2016) 68–85.
[9] S. Bahl, S. Suwas, K. Chatterjee, The control of crystallographic texture in the use of magnesium as a resorbable biomaterial, RSC Adv. 4 (99) (2014) 55677–55684.
[10] Q. Jiang, X. Ma, K. Zhang, Y. Li, X. Li, Y. Li, M. Ma, B. Hou, Anisotropy of the crystallographic orientation and corrosion performance of high-strength AZ80 Mg alloy, J. Magn. Alloys 3 (4) (2015) 309–314.
[11] S. Pawar, T.J.A. Slater, T.L. Burnett, X. Zhou, G.M. Scamans, Z. Fan, G.E. Thompson, P.J. Withers, Crystallographic effects on the corrosion of twin roll cast AZ31 Mg alloy sheet, Acta Mater. 133 (2017) 90–99.
[12] Y.-C. Zhao, G.-S. Huang, G.-G. Wang, T.-Z. Han, F.-S. Pan, Influence of grain orientation on the corrosion behavior of rolled AZ31 magnesium alloy, Acta Metall. Sin. (English Lett.) 28 (11) (2015) 1387–1393.
[13] Z. Pu, G.L. Song, S. Yang, J.C. Outeiro, O.W. Dillon, D.A. Puleo, I.S. Jawahir, Grain refined and basal textured surface produced by burnishing for improved corrosion performance of AZ31B Mg alloy, Corros. Sci. 57 (2012) 192–201.
[14] F. Cao, G.-L. Song, A. Atrens, Corrosion and passivation of magnesium alloys, Corros. Sci. 111 (2016) 835–845.
[15] O.I. Velikokhatnyi, P.N. Kumta, First-principles studies on alloying and simplified thermodynamic aqueous chemical stability of calcium-, zinc-, aluminum-, yttrium- and iron-doped magnesium alloys, Acta Biomater. 6 (5) (2010) 1698–1704.
[16] A. Samaniego, K. Gusieva, I. Llorente, S. Feliu, N. Birbilis, Exploring the possibility of protective surface oxides upon Mg alloy AZ31 via lutetium additions, Corros. Sci. 89 (2014) 101–110.
[17] F. Cao, Z. Shi, G.-L. Song, M. Liu, A. Atrens, Corrosion behaviour in salt spray and in 3.5% nacl solution saturated with Mg(Oh)2 of as-cast and solution heat-treated binary Mg–x alloys: x=Mn, Sn, Ca, Zn, Al, Zr, Si, Sr, Corros. Sci. 76 (2013) 60–97.
[18] F. Cao, Z. Shi, J. Hofstetter, P.J. Uggowitzer, G. Song, M. Liu, A. Atrens, Corrosion of ultra-high-purity Mg in 3.5% NaCl solution saturated with Mg(OH)2, Corros. Sci. 75 (2013) 78–99.
[19] A. Bahmani, Development of High Strength and Corrosion Resistant Magnesium Alloys Using Severe Plastic Deformation Process, Seoul National University, 2018.
[20] N. Birbilis, K.D. Ralston, S. Virtanen, H.L. Fraser, C.H.J. Davies, Grain character influences on corrosion of ECAPed pure magnesium, corrosion engineering, Sci. Technol. 45 (3) (2010) 224–230.
[21] K.D. Ralston, N. Birbilis, C.H.J. Davies, Revealing the relationship between grain size and corrosion rate of metals, Scr. Mater. 63 (12) (2010) 1201–1204.
[22] K.D. Ralston, N. Birbilis, Effect of grain size on corrosion: a review, Corrosion 66 (7) (2010) 075005–075013.
[23] Y. Liu, D. Liu, C. You, M. Chen, Effects of grain size on the corrosion resistance of pure magnesium by cooling rate-controlled solidification, Front Mater. Sci. 9 (3) (2015) 247–253.
[24] G. Han, J.-Y. Lee, Y.-C. Kim, J.H. Park, D.-I. Kim, H.-S. Han, S.-J. Yang, H.-K. Seok, Preferred crystallographic pitting corrosion of pure magnesium in hanks' solution, Corros. Sci. 63 (2012) 316–322.
[25] T. Zheng, Y. Hu, S. Yang, Effect of grain size on the electrochemical behavior of pure magnesium anode, J. Magn. Alloys 5 (2017) 404–411.
[26] T. Kokubo, H. Takadama, How useful is sbf in predicting in vivo bone bioactivity? Biomaterials 27 (15) (2006) 2907–2915.
[27] D. Ahmadkhaniha, A. Jarvenpaa, M. Jaskari, M.H. Sohi, A. Zarei-Hanzaki, M. Fedel, F. Deflorian, L.P. Karjalainen, Microstructural modification of pure mg for improving mechanical and biocorrosion properties, J. Mech. Behav. Biomed. Mater. 61 (2016) 360–370.
[28] D. Ahmadkhaniha, M. Fedel, M. Heydarzadeh Sohi, F. Deflorian, Corrosion behavior of severely plastic deformed magnesium based alloys: a review, Surf. Eng. Appl. Electrochem. 53 (5) (2017) 439–448.
[29] D. Song, A. Ma, J. Jiang, P. Lin, D. Yang, J. Fan, Corrosion behavior of equal-channel-angular-pressed pure magnesium in NaCl aqueous solution, Corros. Sci. 52 (2) (2010) 481–490.
[30] Z. Li, S.-j. Zhou, N. Huang, Effects of ecae processing temperature on the microstructure, mechanical properties, and corrosion behavior of pure Mg, Int. J. Miner. Metall. Mater. 22 (6) (2015) 639–647.
[31] H.A. Johansen, G.B. Adams, P. Van Rysselberghe, Anodic oxidation of aluminum, chromium, hafnium, niobium, tantalum, titanium, vanadium, and zirconium at very low current densities, J. Electrochem. Soc. 104 (1957) 339–346.
[32] A. Balyanov, Corrosion resistance of ultra fine-grained ti, Scr. Mater. 51 (3) (2004) 225–229.
[33] S.G. Wang, C.B. Shen, K. Long, F. Zhang, F.H. Wang, Z.D. Zhang, The electrochemical corrosion of bulk nanocrystalline ingot iron in acidic sulfate solution, J. Phys. Chem. B 110 (2006) 377–382.
[34] H.S. Kim, W.J. Kim, Annealing effects on the corrosion resistance of ultrafine-grained pure titanium, Corros. Sci. 89 (2014) 331–337.
[35] D. Song, A.-b. Ma, J.-h. Jiang, P.-h. Lin, D.-h. Yang, Corrosion behavior of ultra-fine grained industrial pure al fabricated by ECAP, Trans. Nonferrous Metals Soc. China 19 (5) (2009) 1065–1070.
[36] N.N. Aung, W. Zhou, Effect of grain size and twins on corrosion behaviour of AZ31B magnesium alloy, Corros. Sci. 52 (2) (2010) 589–594.
[37] G.R. Argade, S.K. Panigrahi, R.S. Mishra, Effects of grain size on the corrosion resistance of wrought magnesium alloys containing neodymium, Corros. Sci. 58 (2012) 145–151.
[38] J. Liao, M. Hotta, N. Yamamoto, Corrosion behavior of fine-grained AZ31B magnesium alloy, Corros. Sci. 61 (2012) 208–214.
[39] D. Song, A.B. Ma, J.H. Jiang, P.H. Lin, D.H. Yang, J.F. Fan, Corrosion behaviour of bulk ultra-fine grained AZ91D magnesium alloy fabricated by equal-channel angular pressing, Corros. Sci. 53 (1) (2011) 362–373.
[40] M. Ben-Haroush, G. Ben-Hamu, D. Eliezer, L. Wagner, The relation between microstructure and corrosion behavior of AZ80 Mg alloy following different extrusion temperatures, Corros. Sci. 50 (6) (2008) 1766–1778.
[41] M.-K. Chung, Y.-S. Choi, J.-G. Kim, Y.-M. Kim, J.-C. Lee, Effect of the number of ECAP pass time on the electrochemical properties of 1050 al alloys, Materials Science and Engineering: A 366 (2) (2004) 282–291.
[42] S. Gollapudi, Grain size distribution effects on the corrosion behaviour of materials, Corros. Sci. 62 (2012) 90–94.
[43] H.S. Kim, G.H. Kim, H. Kim, W.J. Kim, Enhanced corrosion resistance of high strength Mg-3Al-1Zn alloy sheets with ultrafine grains in a phosphate-buffered saline solution, Corros. Sci. 74 (2013) 139–148.
[44] H.S. Kim, W.J. Kim, Enhanced corrosion resistance of ultrafine-grained AZ61 alloy containing very fine particles of Mg17Al12 phase, Corros. Sci. 75 (2013) 228–238.
[45] A. Bahmani, K.S. Shin, Effect of severe plastic deformation on mechanical properties and corrosion behavior of magnesium alloys, Magn. Technol. (2018) 369–371.
[46] E. Mostaed, M. Vedani, M. Hashempour, M. Bestetti, Influence of ECAP process on mechanical and corrosion properties of pure Mg and ZK60 magnesium alloy for biodegradable stent applications, Biomatter 4 (2014) e28283.
[47] E. Mostaed, M. Hashempour, A. Fabrizi, D. Dellasega, M. Bestetti, F. Bonollo, M. Vedani, Microstructure, texture evolution, mechanical properties and corrosion behavior of ecap processed ZK60 magnesium alloy for biodegradable applications, J. Mech. Behav. Biomed. Mater. 37 (2014) 307–322.
[48] F.S.J. Poggiali, C.L.P. Silva, P.H.R. Pereira, R.B. Figueiredo, P.R. Cetlin, Determination of mechanical anisotropy of magnesium processed by ECAP, J. Mater. Res. Technol. 3 (4) (2014) 331–337.

[49] Y. Yuan, A. Ma, X. Gou, J. Jiang, G. Arhin, D. Song, H. Liu, Effect of heat treatment and deformation temperature on the mechanical properties of ECAP processed ZK60 magnesium alloy, Mater. Sci. Eng.: A 677 (Supplement C) (2016) 125–132.
[50] P. Minárik, J. Veselý, R. Král, J. Bohlen, J. Kubásek, M. Janeček, J. Stráská, Exceptional mechanical properties of ultra-fine grain mg-4y-3re alloy processed by ECAP, Mater. Sci. Eng.: A 708 (Supplement C) (2017) 193–198.
[51] A.M. Jorge Jr, E. Prokofiev, M.R.M. Triques, V. Roche, W.J. Botta, C.S. Kiminami, G.I. Raab, R.Z. Valiev, T.G. Langdon, Effect of cold rolling on the structure and hydrogen properties of AZ91 and AM60D magnesium alloys processed by ECAP, Int. J. Hydrogen Energy 42 (34) (2017) 21822–21831.
[52] Y.S. Kim, E. Choi, W.J. Kim, Characterization of the microstructures and the shape memory properties of the Fe-Mn-Si-Cr-Ni-c shape memory alloy after severe plastic deformation by differential speed rolling and subsequent annealing, Mater. Charact. 136 (2018) 12–19.
[53] M.G. Kim, J.K. Kim, H.S. Kim, W.J. Kim, J.H. Han, Effect of post-annealing and strong deformation process on the mechanical and corrosion properties of a Mg-Mn alloy for biomedical application, J. Korean Phys. Soc. 72 (6) (2018) 692–698.
[54] W.J. Kim, J.B. Lee, W.Y. Kim, H.T. Jeong, H.G. Jeong, Microstructure and mechanical properties of Mg–Al–Zn alloy sheets severely deformed by asymmetrical rolling, Scr. Mater. 56 (4) (2007) 309–312.
[55] A. Nikfahm, I. Danaee, A. Ashrafi, M.R. Toroghinejad, Effect of grain size changes on corrosion behavior of copper produced by accumulative roll bonding process, Mater. Res. 16 (2013) 1379–1386.
[56] M. Karimi, M.R. Toroghinejad, J. Dutkiewicz, Nanostructure formation during accumulative roll bonding of commercial purity titanium, Mater. Charact. 122 (Supplement C) (2016) 98–103.
[57] A. Mashhadi, A. Atrian, L. Ghalandari, Mechanical and microstructural investigation of Zn/Sn multilayered composites fabricated by accumulative roll bonding (ARB) process, J. Alloys Compd. 727 (Supplement C) (2017) 1314–1323.
[58] M.R. Morovvati, B.M. Dariani, The effect of annealing on the formability of aluminum 1200 after accumulative roll bonding, J. Manuf. Process. 30 (Supplement C) (2017) 241–254.
[59] S.M. Fatemi-Varzaneh, A. Zarei-Hanzaki, Processing of AZ31 magnesium alloy by a new noble severe plastic deformation method, Mater. Sci. Eng.: A 528 (3) (2011) 1334–1339.
[60] S. Asqardoust, A. Zarei Hanzaki, H.R. Abedi, T. Krajnak, P. Minárik, Enhancing the strength and ductility in accumulative back extruded WE43 magnesium alloy through achieving bimodal grain size distribution and texture weakening, Mater. Sci. Eng.: A 698 (Supplement C) (2017) 218–229.
[61] S.M. Fatemi-Varzaneh, A. Zarei-Hanzaki, Accumulative back extrusion (ABE) processing as a novel bulk deformation method, Mater. Sci. Eng.: A 504 (1) (2009) 104–106.
[62] H. Alihosseini, G. Faraji, A.F. Dizaji, K. Dehghani, Characterization of ultra-fine grained aluminum produced by accumulative back extrusion (ABE), Mater. Charact. 68 (Supplement C) (2012) 14–21.
[63] N. Haghdadi, A. Zarei-Hanzaki, H.R. Abedi, D. Abou-Ras, M. Kawasaki, A.P. Zhilyaev, Evolution of microstructure and mechanical properties in a hypoeutectic Al-Si-Mg alloy processed by accumulative back extrusion, Mater. Sci. Eng.: A 651 (Supplement C) (2016) 269–279.
[64] M. Diez, H.-E. Kim, V. Serebryany, S. Dobatkin, Y. Estrin, Improving the mechanical properties of pure magnesium by three-roll planetary milling, Mater. Sci. Eng.: A 612 (2014) 287–292.
[65] Y.-M. Hwang, W.M. Tsai, F.H. Tsai, I. Her, Analytical and experimental study on the spiral marks of the rolled product during three-roll planetary rolling processes, Int. J. Mach. Tools Manuf. 46 (12–13) (2006) 1555–1562.
[66] Y. Li Wang, A. Molotnikov, M. Diez, R. Lapovok, H.-E. Kim, J. Tao Wang, Y. Estrin, Gradient structure produced by three roll planetary milling: numerical simulation and microstructural observations, Mater. Sci. Eng.: A 639 (Supplement C) (2015) 165–172.
[67] T.S. Mahmoud, Effect of friction stir processing on electrical conductivity and corrosion resistance of AA6063-T6 al alloy, proceedings of the institution of mechanical engineers, Part C: J. Mech. Eng. Sci. 222 (7) (2008) 1117–1123.
[68] Y.H. Jang, S.S. Kim, C.D. Yim, C.G. Lee, S.J. Kim, Corrosion behaviour of friction stir welded AZ31B Mg in 3·5%NaCl solution, corrosion engineering, Sci. Technol. 42 (2) (2013) 119–122.
[69] G. Rambabu, D. Balaji Naik, C.H. Venkata Rao, K. Srinivasa Rao, G. Madhusudan Reddy, Optimization of friction stir welding parameters for improved corrosion resistance of AA2219 aluminum alloy joints, Def. Technol. 11 (4) (2015) 330–337.
[70] B. Ratna Sunil, G. Pradeep Kumar Reddy, Corrosion behavior of friction stir welded AZ31B Mg alloy - Al6063 alloy joint, Cogent Eng. 3 (1) (2016) 1145565.
[71] J.H. Gao, S.K. Guan, Z.W. Ren, Y.F. Sun, S.J. Zhu, B. Wang, Homogeneous corrosion of high pressure torsion treated Mg–Zn–Ca alloy in simulated body fluid, Mater. Lett. 65 (4) (2011) 691–693.
[72] Y. Ivanisenko, R. Kulagin, V. Fedorov, A. Mazilkin, T. Scherer, B. Baretzky, H. Hahn, High pressure torsion extrusion as a new severe plastic deformation process, Mater. Sci. Eng.: A 664 (Supplement C) (2016) 247–256.
[73] X. Wang, M. Nie, C.T. Wang, S.C. Wang, N. Gao, Microhardness and corrosion properties of hypoeutectic Al-7Si alloy processed by high-pressure torsion, Mater. Des. 83 (Supplement C) (2015) 193–202.
[74] A. Hohenwarter, Incremental high pressure torsion as a novel severe plastic deformation process: processing features and application to copper, Mater. Sci. Eng.: A 626 (Supplement C) (2015) 80–85.
[75] X. Yang, H. Miura, T. Sakai, Structural development at severely high strain in AZ31 magnesium alloy processed by cold forging and subsequent annealing, Mater. Des. 44 (2013) 573–579.
[76] H. Miura, G. Yu, X. Yang, Multi-directional forging of AZ61Mg alloy under decreasing temperature conditions and improvement of its mechanical properties, Mater. Sci. Eng.: A 528 (22–23) (2011) 6981–6992.
[77] J. Li, J. Liu, Z. Cui, Microstructures and mechanical properties of AZ61 magnesium alloy after isothermal multidirectional forging with increasing strain rate, Mater. Sci. Eng.: A 643 (Supplement C) (2015) 32–36.
[78] M.R. Jandaghi, H. Pouraliakbar, M.K.G. Shiran, G. Khalaj, M. Shirazi, On the effect of non-isothermal annealing and multi-directional forging on the microstructural evolutions and correlated mechanical and electrical characteristics of hot-deformed Al-Mg alloy, Mater. Sci. Eng.: A 657 (Supplement C) (2016) 431–440.
[79] C. Cai, S. LingHui, D. XingHao, W. BaoLin, Enhanced mechanical property of AZ31B magnesium alloy processed by multi-directional forging method, Mater. Charact. 131 (2017) 72–77.
[80] B. Wang, C. Liu, Y. Gao, S. Jiang, Z. Chen, Z. Luo, Microstructure evolution and mechanical properties of Mg-Gd-Y-Ag-Zr alloy fabricated by multidirectional forging and ageing treatment, Mater. Sci. Eng.: A 702 (2017) 22–28.
[81] H. Miura, T. Maruoka, J.J. Jonas, Effect of ageing on microstructure and mechanical properties of a multi-directionally forged Mg-6al-1 Zn alloy, Mater. Sci. Eng.: A 563 (2013) 53–59.
[82] Y. Uematsu, T. Kakiuchi, H. Miura, T. Nozaki, Effect of grain size on fatigue behavior in AZ61 Mg alloys fabricated by MDFing, Mater. Trans. 57 (9) (2016) 1454–1461.
[83] X. Liu, L. Xiao, C. Wei, X. Xu, M. Luo, W. Yan, Effect of multi-directional forging and annealing on abrasive wear behavior in a medium carbon low alloy steel, Tribol. Int. 119 (2018) 608–613.
[84] R. Zhang, D. Wang, S. Yuan, Effect of multi-directional forging on the microstructure and mechanical properties of Tibw/ta15 composite with network architecture, Mater. Des. 134 (Supplement C) (2017) 250–258.
[85] A. Atrens, G.-L. Song, M. Liu, Z. Shi, F. Cao, M.S. Dargusch, Review of recent developments in the field of magnesium corrosion, Adv. Eng. Mater. 17 (4) (2015) 400–453.
[86] F. Cao, Z. Shi, G.-L. Song, M. Liu, M.S. Dargusch, A. Atrens, Influence of hot rolling on the corrosion behavior of several Mg-x alloys, Corros. Sci. 90 (2015) 176–191.

[87] Z. Shi, F. Cao, G.-L. Song, M. Liu, A. Atrens, Corrosion behaviour in salt spray and in 3.5% nacl solution saturated with Mg(oh)2 of as-cast and solution heat-treated binary Mg-Re alloys: rE=Ce, la, Nd, Y, Gd, Corros. Sci. 76 (2013) 98–118.
[88] A. Atrens, M. Liu, N.I. Zainal Abidin, Corrosion mechanism applicable to biodegradable magnesium implants, Mater. Sci. Eng.: B 176 (20) (2011) 1609–1636.
[89] C.D. Lee, C.S. Kang, K.S. Shin, Effect of galvanic corrosion between precipitate and matrix on corrosion behaviour of As-cast Mg-Al alloys, Met. Mater. 6 (2000) 351–358.
[90] W. Melitz, J. Shen, A.C. Kummel, S. Lee, Kelvin probe force microscopy and its application, Surf. Sci. Rep. 66 (1) (2011) 1–27.
[91] A. Sadeghi, E. Hasanpur, A. Bahmani, K.S. Shin, Corrosion behaviour of AZ31 magnesium alloy containing various levels of strontium, Corros. Sci. 141 (2018) 117–126.
[92] A. Bahmani, S. Arthanari, K.S. Shin, Improved corrosion resistant and strength of a magnesium alloy using multi-directional forging (MDF), Int. J. Adv. Manuf. Technol. (2019).
[93] I. Apachitei, L.E. Fratila-Apachitei, J. Duszczyk, Microgalvanic activity of an Mg-Al-Ca-based alloy studied by scanning kelvin probe force microscopy, Scr. Mater. 57 (11) (2007) 1012–1015.
[94] A.E. Coy, F. Viejo, P. Skeldon, G.E. Thompson, Susceptibility of rare-earth-magnesium alloys to micro-galvanic corrosion, Corros. Sci. 52 (12) (2010) 3896–3906.
[95] R. Arrabal, A. Pardo, M.C. Merino, M. Mohedano, P. Casajús, K. Paucar, G. Garcés, Effect of nd on the corrosion behaviour of AM50 and AZ91D magnesium alloys in 3.5 wt.% Nacl solution, Corros. Sci. 55 (2012) 301–312.
[96] G. Ben-Hamu, D. Eliezer, C.E. Cross, T. Böllinghaus, The relation between microstructure and corrosion behavior of GTA welded AZ31B magnesium sheet, Mater. Sci. Eng.: A 452-453 (2007) 210–218.
[97] M.C. Merino, A. Pardo, R. Arrabal, S. Merino, P. Casajús, M. Mohedano, Influence of chloride ion concentration and temperature on the corrosion of Mg-Al alloys in salt fog, Corros. Sci. 52 (5) (2010) 1696–1704.
[98] R. Arrabal, A. Pardo, M.C. Merino, K. Paucar, M. Mohedano, P. Casajús, G. Garcés, Influence of Gd on the corrosion behavior of AM50 and AZ91D magnesium alloys, Corrosion 68 (5) (2012) 398–410.
[99] T. Cain, L.G. Bland, N. Birbilis, J.R. Scully, A compilation of corrosion potentials for magnesium alloys, Corrosion 70 (10) (2014) 1043–1051.
[100] M. Mohedano, R. Arrabal, Á. Pardo, M.C. Merino, K. Paucar, P. Casajús, E. Matykina, Salt spray corrosion behaviour of new Mg-Al alloys containing nd or gd, corrosion engineering, Sci. Technol. 48 (3) (2013) 183–193.
[101] R. Arrabal, B. Mingo, A. Pardo, E. Matykina, M. Mohedano, M.C. Merino, A. Rivas, A. Maroto, Role of alloyed Nd in the microstructure and atmospheric corrosion of as-cast magnesium alloy AZ91, Corros. Sci. 97 (2015) 38–48.
[102] R. Arrabal, E. Matykina, A. Pardo, M.C. Merino, K. Paucar, M. Mohedano, P. Casajús, Corrosion behaviour of AZ91D and AM50 magnesium alloys with Nd and Gd additions in humid environments, Corros. Sci. 55 (2012) 351–362.
[103] J. Liu, Y. Song, J. Chen, P. Chen, D. Shan, E.-H. Han, The special role of anodic second phases in the micro-galvanic corrosion of EW75 Mg alloy, Electrochim. Acta 189 (2016) 190–195.
[104] G. Ben-Hamu, D. Eliezer, K.S. Shin, The role of si and Ca on new wrought Mg-Zn-Mn based alloy, Mater. Sci. Eng.: A 447 (1–2) (2007) 35–43.
[105] W. Liu, F. Cao, A. Chen, L. Chang, J. Zhang, C. Cao, Corrosion behaviour of AM60 magnesium alloys containing ce or la under thin electrolyte layers. Part 1: microstructural characterization and electrochemical behaviour, Corros. Sci. 52 (2) (2010) 627–638.
[106] S.-M. Baek, J.S. Kang, H.-J. Shin, C.D. Yim, B.S. You, H.-Y. Ha, S.S. Park, Role of alloyed y in improving the corrosion resistance of extruded Mg-Al-Ca-based alloy, Corros. Sci. 118 (2017) 227–232.
[107] A. Bahmani, S. Arthanari, K.S. Shin, Corrosion behavior of Mg-Mn-Ca alloy: influences of Al, Sn and Zn, J. Magn. Alloys 7 (1) (2019) 38–46.
[108] G. Williams, K. Gusieva, N. Birbilis, Localized corrosion of binary mg-nd alloys in chloride-containing electrolyte using a scanning vibrating electrode technique, Corrosion 68 (6) (2012) 489–498.
[109] F. Andreatta, I. Apachitei, A.A. Kodentsov, J. Dzwonczyk, J. Duszczyk, Volta potential of second phase particles in extruded AZ80 magnesium alloy, Electrochim. Acta 51 (17) (2006) 3551–3557.
[110] W. Liu, F. Cao, A. Chen, L. Chang, J. Zhang, C. Cao, Effect of chloride ion concentration on electrochemical behavior and corrosion product of AM60 magnesium alloy in aqueous solutions, Corrosion 68 (2012) 045001-1, 045001-13.
[111] S. Abbasi, M. Aliofkhazraei, H. Mojiri, M. Amini, M. Ahmadzadeh, M. Shourgeshty, Corrosion behavior of pure mg and AZ31 magnesium alloy, Protect. Metals Phys. Chem. Surf. 53 (3) (2017) 573–578.
[112] J. Przondziono, W. Walke, J. Szala, E. Hadasik, J. Wieczorek, Evaluation of corrosion resistance of casting magnesium alloy AZ31 in NaCl solutions, IOP Conf. Ser.: Mater. Sci. Eng. 22 (2011) 012017.
[113] L. Li, Q. Qu, W. Bai, Y. Chen, S. Zhang, G. Gao, Z. Ding, Effect of nacl on the corrosion of cold rolled steel in peracetic acid solution, Int. J. Electrochem. Sci. Technol. Adv. Mater. 7 (2012) 3773–3786.
[114] K.M. Emran, Effects of concentration and temperature on the corrosion properties of the Fe-Ni-Mn alloy in HCl solutions, Res. Chem. Intermed. 41 (6) (2013) 3583–3596.
[115] N. Birbilis, M.A. Easton, A.D. Sudholz, S.M. Zhu, M.A. Gibson, On the corrosion of binary magnesium-rare earth alloys, Corros. Sci. 51 (3) (2009) 683–689.
[116] A. Atrens, G.-L. Song, F. Cao, Z. Shi, P.K. Bowen, Advances in mg corrosion and research suggestions, J. Magn. Alloys 1 (3) (2013) 177–200.
[117] F. Cao, Corrosion and stress corrosion cracking of magnesium alloys Ph.D. Thesis, The University of Queensland, 2015.
[118] S.-M. Baek, H.J. Kim, H.Y. Jeong, S.-D. Sohn, H.-J. Shin, K.-J. Choi, K.-S. Lee, J.G. Lee, C.D. Yim, B.S. You, H.-Y. Ha, S.S. Park, Effect of alloyed Ca on the microstructure and corrosion properties of extruded AZ61 Mg alloy, Corros. Sci. 112 (2016) 44–53.
[119] Y.S. Jeong, W.J. Kim, Enhancement of mechanical properties and corrosion resistance of Mg-Ca alloys through microstructural refinement by indirect extrusion, Corros. Sci. 82 (2014) 392–403.
[120] A. Bahmani, S. Arthanari, K.S. Shin, Improvement of corrosion resistance and mechanical properties of a magnesium alloy using screw rolling, J. Alloys Compd. 813 (2020) 152155.
[121] A. Bahmani, K.S. Shin, Effects of Severe Plastic Deformation on Mechanical Properties and Corrosion Behavior of Magnesium Alloys, Springer International Publishing, Cham, 2018, pp. 369–371.